ACS APPLIED MATERIALS & INTERFACES

Research Article

www.acsami.org

# Laterally-Stacked, Solution-Processed Organic Microcrystal With Ambipolar Charge Transport Behavior

Hyunseok Shim,† Amit Kumar,† Hyejin Cho, Dongmyung Yang, Akshaya K. Palai, and Seungmoon Pyo*

Department of Chemistry, Konkuk University, 120 Neungdong-ro, Gwangjin-gu, Seoul 143-701, Republic of Korea

Supporting Information

**ABSTRACT:** We report the formation of laterally stacked ambipolar crystal wire for high-mobility organic field-effect transistors (OFETs), along with a simple logic circuit through a solution process. A soluble pentacene derivative, 6,13-bis(triisopropylsilylethynyl)pentacene (Tips-pentacene), and N,N′-dioctyl-3,4,9,10-perylenedicarboximide (PTCDI-$C_8$) were used as p-type and n-type organic semiconductors, respectively. The laterally stacked ambipolar crystal wire is made up of Tips-pentacene and PTCDI-$C_8$ crystals in a structure of Tips-pentacene/PTCDI-$C_8$/Tips-pentacene (TPT). The inner part of the crystal is made up of PTCDI-$C_8$, and Tips-pentacene is present on both sides. These TPT crystals exhibit typical ambipolar charge transport behavior in organic electronic devices, which show very balanced hole and electron mobility as high as 0.23 $cm^2/V{\cdot}s$ and 0.13 $cm^2/V{\cdot}s$, respectively. Static and dynamic operational stability of the device is investigated by measuring the device performance as a function of storage time and applying voltage pulse, respectively, and it shows good air stability. In addition, a simple logic circuit based on the TPT crystal wire has been fabricated, and the static and dynamic performance has been evaluated. The results indicate that the TPT crystals are potentially useful for miniaturized organic electronic devices.

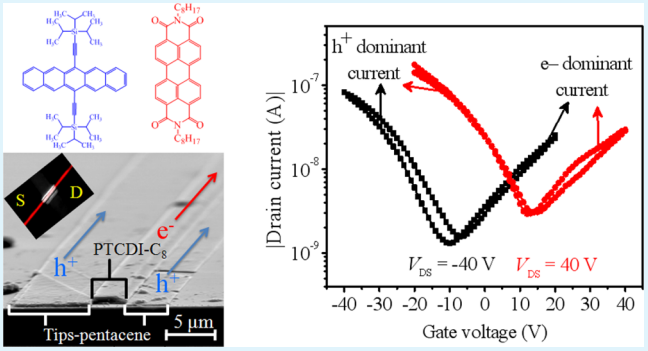


**KEYWORDS:** *organic crystal, organic semiconductor, organic field-effect transistor, organic gate dielectric, organic inverter*

## INTRODUCTION

Ambipolar organic field-effect transistors (ambi-OFETs) with balanced carrier (electrons and holes) mobility have attracted enormous attention because of their potential applications in advanced organic electronic devices such as organic light-emitting transistors and complementary-like organic circuits.[1−3] Ambi-OFETs can be fabricated using one ambipolar material[4,5] or by combining two unipolar materials (p- and n-type).[6,7] The fabrication of highly efficient ambipolar devices using one ambipolar organic material is still being researched, because achieving balanced p- and n-type charge transport in ambient conditions is very difficult with one organic material. High-efficiency ambi-OFETs are generally fabricated by combining p- and n-type semiconductors.[8] Various heterostructures such as bulk heterojunctions,[9,10] bilayer heterojunctions,[11,12] and lateral heterostructures[13] are formed by combining p- and n-type semiconductors. In the bulk heterojunction structures, no direct channel can be formed, and it makes charge transport mechanism more complicated. In the bilayer structure in which only one semiconductor (either p- or n-type) is in direct contact with electrodes, channel can be formed at two different interfaces such as semiconductor/gate dielectric and semiconductor/semiconductor interface.[14] In those structures, to achieve balanced charge transport of hole and electron is very critical issue.

Very recently, researchers have developed cocrystallization or coassembly techniques to obtain active layer with ambipolar charge transport behavior using donor (D) and acceptor (A) molecules. Most charge-transfer (CT) complexes investigated show unconventional metallic (super) conductivities,[15,16] but very recently, theoretical and experimental results revealed that mixed stacked D-A-based charge transfer complexes possess ferro-electricity[17] and ambipolar semiconductivity.[18−20]

Park et al.[21] demonstrated ambipolar charge transport with hole and electron mobilities of $6.7 \times 10^{-3}$ $cm^2/V{\cdot}s$ and $6.7 \times 10^{-2}$ $cm^2/V{\cdot}s$, respectively, in a mixed stacked charge transfer complex crystal by using 4M-DSB as a donor and CN-TFPA as an acceptor molecule. Sulfur-bridged annulene cocrystal systems ($C_{60}$-DPTTA, $C_{70}$-DPTTA, and TCNQ-DPTTA) studied by Zhang et al.[22,23] also showed ambipolar charge transport with electron and hole mobility ranging from $10^{-3}$ to $10^{-2}$ $cm^2/V{\cdot}s$. Wu et al.[24] took the charge transfer characteristics between D and A molecules and reported cocrystal microrods of dibenzotetrathiafulvalene and tetracyanoquinodimethane with ambipolar charge carrier mobility values of 0.04 $cm^2/V$ s and 0.13 $cm^2/V{\cdot}s$ for holes and electrons, respectively.

Received: July 8, 2014
Accepted: September 22, 2014
Published: September 22, 2014

  

In spite of the ambipolar charge transporting behavior of CT crystal, some drawbacks are associated with the fabrication of well-balanced high-mobility ambipolar devices. First, careful selection of the D and A molecules is required to achieve an efficient CT cocrystal system, because the electronic properties of the CT structures are driven by their frontier molecular orbital and their specific molecular arrangement. Therefore, very few reports are available on such ambipolar CT cocrystals. Example of CT cocrystal systems includes bis(ethylenedithio) (BEDT) substituted tetrathiafulvalene (TTF) as a donor and tetracyanoquinodimethane (TCNQ) as an acceptor.[25] Another class of such compounds is fullerene and porphyrin hybrid nanosheets in which fullerene acts as donor moiety and cobalt porphyrin acts as acceptor reported by Anthopoulos et al., and it shows ambipolar charge transport.[26] Second, charge transport in the CT systems depends on the temperature. For example, a (BEDT-TTF)($F_2$TCNQ) based crystal exhibits ambipolar charge transport only at low temperatures (2−60 K) with mobilities of about $10^{-3}$ $cm^2/V{\cdot}s$.[27] Takahashi et al. reported ambipolar charge transport in a DBTTF-TCNQ crystal (prepared by cosublimation) by using specific Fermi-level tuned electrodes.[28,29]

Hence, there is a need to provide an alternative and easy way for the fabrication of ambipolar crystal with high and balanced charge carrier mobility under ambient conditions. Balanced ambipolar charge transport in the devices can be obtained by placing both n- and p-type organic semiconductors in direct contact with the source/drain in a highly ordered manner. Tang et al.[30] fabricated highly balanced ambi-OFET with hole and electron mobilities of 0.1 and 0.17 $cm^2/V{\cdot}s$, respectively, by placing individual crystalline ribbons of CuPc and $F_{16}$CuPc side by side in between source and drain electrodes in a mechanical way. Although very balanced hole and electron mobilities have been achieved, this technique needs relatively complicated techniques. Keeping this in mind, we developed a new concept for the formation of a high-quality laterally stacked ambipolar crystal wire through a simple solution process.

The preparation of microwire by a unique solution-based approach called the "capillary tube method" has already been established by our group.[31,32] So far, we have fabricated unipolar 1D-microwire (either p- or n-type) using this method.[33,34] In particular, a single-crystalline ordered crystal array of pure PTCDI-$C_8$ in the presence of a capillary tube from the solution is explained in detail in our previous publications,[33] where the unidirectional crystal growth mechanism was discussed and the single-crystalline nature of PTCDI-$C_8$ microstructure was studied by 2D-GIXD measurement. In view of its excellent unidirectional crystal-forming tendency, we used PTCDI-$C_8$ in combination with Tips-pentacene in order to make high quality laterally stacked ambipolar crystal wire.

In this work, we report on the very easy solution-based direct formation of a laterally stacked ambipolar crystals of Tips-pentacene and PTCDI-$C_8$ [Tips-pentacene/PTCDI-$C_8$/Tips-pentacene (TPT) type] with sufficient length by optimizing the solution concentration of Tips-pentacene (p-type) and PTCDI-$C_8$ (n-type). These ambipolar crystals were incorporated in constructing top-contact, bottom-gate ambi-OFETs and inverters with a cross-linked poly(4-vinylphenol) gate dielectric. Since both the p- and n-type semiconductors are in direct contact with source and drain electrodes in our system, we expect the direct injection of respective charge carriers from the electrode for a device with highly balanced and efficient ambipolar charge transport.

The electrical responses of the ambi-OFETs, load- and complementary-type inverter were investigated in detail. The OFETs show ambipolar charge transport in ambient conditions with very high and well-balanced electron (0.12 $cm^2/V{\cdot}s$) and hole (~0.2 $cm^2/V{\cdot}s$) charge carrier transport behavior. The devices show good static and dynamic operational stability in air, and a decent voltage transfer characteristic of the load and complementary-type inverter is also observed.

## EXPERIMENTAL SECTION

Top-contact and bottom gate geometry was employed for the fabrication of OFETs. The materials for this study include PTCDI-$C_8$, Tips-pentacene, poly(4-vinylphenol) (PVP), poly(melamine-*co*-formaldehyde), and propylene glycol monomethyl ether acetate, which were purchased from Aldrich Chemical Co. and used as supplied without further purification. Devices were fabricated on an indium−tin oxide (ITO)-coated glass substrate with a sheet resistance of ~20 $\Omega/cm^2$ as a gate electrode, which was patterned and cleaned through an electronic cleaning process.[31] Cross-linked poly(4-vinylphenol) (CL-PVP) was used as the gate dielectric and prepared by mixing poly(4-vinylphenol) (10 wt %) and poly(melamine-*co*-formaldehyde) (5 wt %) in propylene glycol monomethyl ether acetate (85 wt %) solution according to a known method.[32]

Ambipolar crystals (TPT type) were formed by dropping a solution onto a capillary tube and dried in ambient conditions established in our laboratory.[31,32] Five types of solutions with different weight ratios of p- to n-type organic semiconductors were prepared. For the preparation of 1:1 (p:n) weight ratio solution, 0.5 mg of Tips-pentacene, and 0.5 mg of PTCDI-$C_8$ was dissolved in 1 mL 1,2-dichlorobenzene. Similarly, 0.2 mg of Tips-pentacene with 0.5 mg of PTCDI-$C_8$, 0.1 mg of Tips-pentacene with 0.5 mg of PTCDI-$C_8$, 0.1 mg of Tips-pentacene with 0.75 mg of PTCDI-$C_8$, and 0.1 mg Tips-pentacene with 1.0 mg of PTCDI-$C_8$ were dissolved in 1 mL of 1,2-dichlorobenzene, respectively, to make 1:2.5, 1:5, 1:7.5, and 1:10 weight ratio solutions. Capillary tubes with outer diameter 1.2 mm, cleaned using acetone and isopropyl alcohol in ultrasonic bath, were placed on the substrate with its length parallel to the patterned bottom ITO electrode. The prepared solutions were added dropwise (5−10 $\mu$L) on the capillary tube and then baked on a hot plate at 90 °C for 1 h in ambient conditions.

A shadow mask was used during the Au source and drain electrode deposition. When ambipolar crystal was used in the active layer, the channel length ($L$) was 50 $\mu$m, and the width ($W$) was calculated as the sum of the width of microcrystals lying in the channel region. Polarized optical microscopy (Olympus BX 51) was used to calculate the microcrystal width. A fluorescence microscope (FM) was used to distinguish the individual widths of the crystals. A scanning electron microscopy (SEM) image was obtained using a TESCAN FESEM MIRA II instrument. Electrical characterization of the devices was performed using an HP semiconductor parameter analyzer (HP 4156A) in ambient conditions. The hole and electron mobilities were calculated in the saturation region using the following formula:

$$I_{DS} = (W/2L)C_i\mu(V_{GS} - V_T)^2$$

where $I_{DS}$ is the drain-source current, $\mu$ is the field-effect mobility, $V_{GS}$ is the gate voltage, $V_T$ is the threshold voltage, and $W$ and $L$ are the width and length of the channel, respectively. Ultraviolet visible near-infrared spectra are recorded using Jasco V-670 and Varian Cary 500 spectrophotometer. X-ray diffraction analysis of unipolar and ambipolar crystals was carried out using an incident X-ray with wavelength of 0.154 nm (PANalytical Empyrean XRD). Differential scanning calorimetry (DSC) measurements (Diamond DSC, PerkinElmer) of the materials were performed with under $N_2$ gas at a heating rate of 10 °C/min.

## RESULTS AND DISCUSSION

The growth of laterally stacked TPT type ambipolar crystal using Tips-pentacene (p-type), PTCDI-$C_8$ (n-type) is

schematically depicted in Figure 1a along with the chemical structure of the semiconductors. The schematics of the device structure of ambi-OFETs, load- and complementary-type inverter based on the ambipolar crystal are shown in Figure 1(b and c, respectively).

For the direct formation of the ambipolar crystal over a substrate, a mixture solution of Tips-pentacene and PTCDI-$C_8$ in 1,2-dichlorobenzene was dropped on a capillary tube and allowed to crystallize in heating conditions (90 °C on a hot plate for 1 h) as shown in Figure 1a. The laterally stacked TPT type ambipolar crystals were formed from the edge of the solution to normal of the tube. Figure 2a shows an optical microscopic (OM) image of the crystals formed in the presence of capillary tube and are found to be highly directional in nature. The inset of the figure shows the magnified image of one of the so formed directional crystal featuring laterally stacked ambipolar crystal wire. On the other hand, when the mixture solution was dropped on a substrate in the absence of capillary tube, the crystals formed are randomly orientated and the shape is not uniform and significantly different from that of crystal formed from capillary tube method [Figure 2b]. It indicates that placing the tube is a necessary step for the formation of highly directional TPT ambipolar crystals. The shape and composition of crystal formed with and without the tube has been investigated by fluorescence microscope, and the images are shown in Figure 2(c–h), which are discussed in detail in a later section.

We also found that the shape and the number of the crystal vary according to the weight ratio of PTCDI-$C_8$ (n-type) to Tips-pentacene (p-type) in solution, as shown in Figures S1(a–e) (Supporting Information with detailed discussion). Only at weight ratios of 1:5, 1:7.5, and 1:10, the laterally stacked TPT ambipolar crystals are formed. The possible mechanism for the formation of the TPT type crystals is that crystals of PTCDI-$C_8$ may form first and act as a seed providing thermodynamically more stable site for Tips-pentacene molecules, resulting in laterally stacked TPT type crystal. However, at other weight ratios, the number of PTCDI-$C_8$ crystals may be relatively less and hence Tips-pentacene molecules may not find the PTCDI-$C_8$ crystal, leading to the other types of crystal instead of TPT type.

The laterally stacked TPT type ambipolar crystal prepared from the solution method is consisted of Tips-pentacene and PTCDI-$C_8$, which are laterally stacked as shown in Figure 2a. To confirm the structural feature and coexistence of PTCDI-$C_8$ and Tips-pentacene in the TPT crystal was characterized by X-ray diffraction analysis and compared with the XRD spectra of pure (unipolar) Tips-pentacene and PTCDI-$C_8$ crystals grown by the same method. The XRD patterns of TPT ambipolar crystal and unipolar crystals are given in Figure 3a.

In case of pure Tips-pentacene crystal, the XRD pattern showed intense peaks at $2\theta$ = 5.39, 10.73, and 16.08°, which are indexed as (001), (002), and (003), respectively, and are consistent with the reported values in the literature.[35] Also, the strong peak at $2\theta$ = 4.45° in XRD pattern of pure PTCDI-$C_8$ can be indexed (001), which is also consistent with the reported values in the literature.[36] In the XRD spectrum of ambipolar crystal, all the peaks correspond to those from the indivisual spectra of Tips-pentacene and PTCDI-$C_8$ with no additional peaks, indicating the presence of both semiconductor without any interaction between them such as charge transfer. It is reported that the XRD pattern for charge transfer

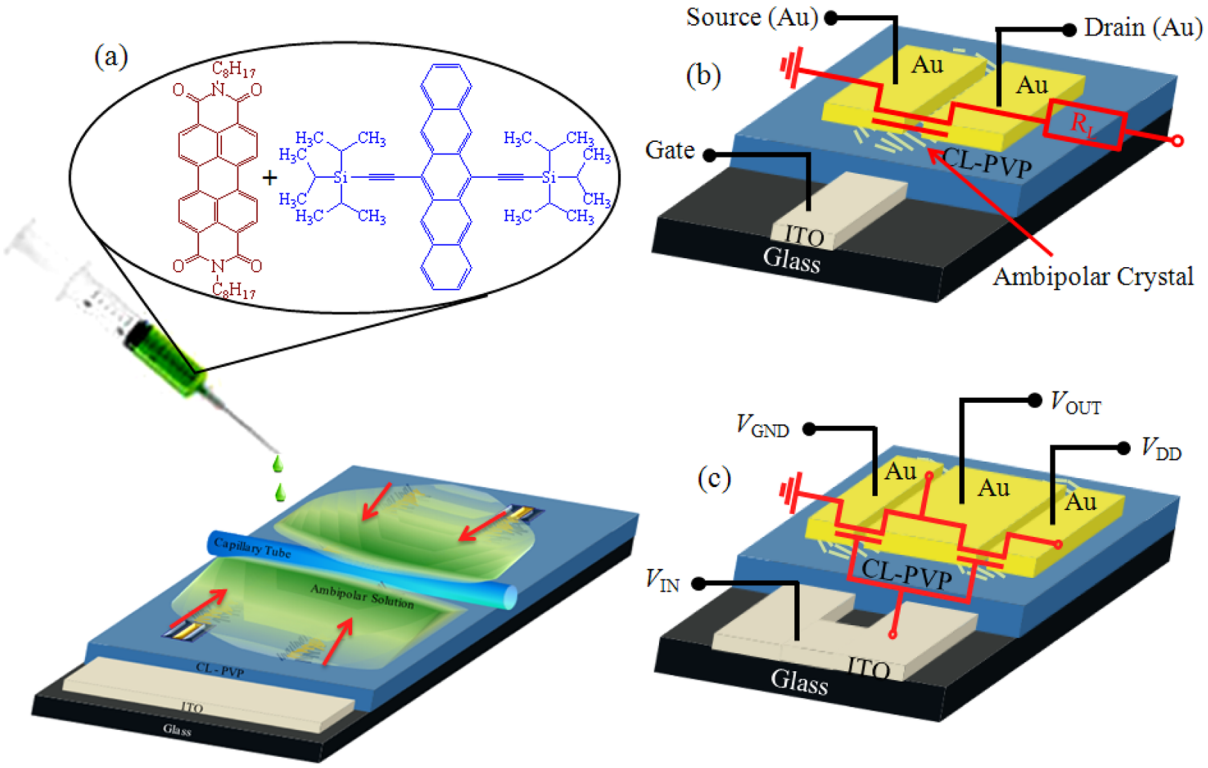


**Figure 1.** (a) Molecular structure of PTCDI-$C_8$ and Tips-pentacene and schematic of device fabrication using a capillary tube. A capillary tube is placed on top of a dielectric film with its length parallel to patterned ITO gate electrode, and a solution containing both Tips-pentacene and PTCDI-$C_8$ is dropped from a syringe onto the tube. The substrate is placed on a hot plate and baked under ambient conditions at 90 °C for 1 h. Gold is deposited using different patterned masks for source/drain deposition to fabricate the (b) OFET and (c) CMOS-like inverter.


dx.doi.org/10.1021/am5044505 | ACS Appl. Mater. Interfaces 2014, 6, 17804–17814

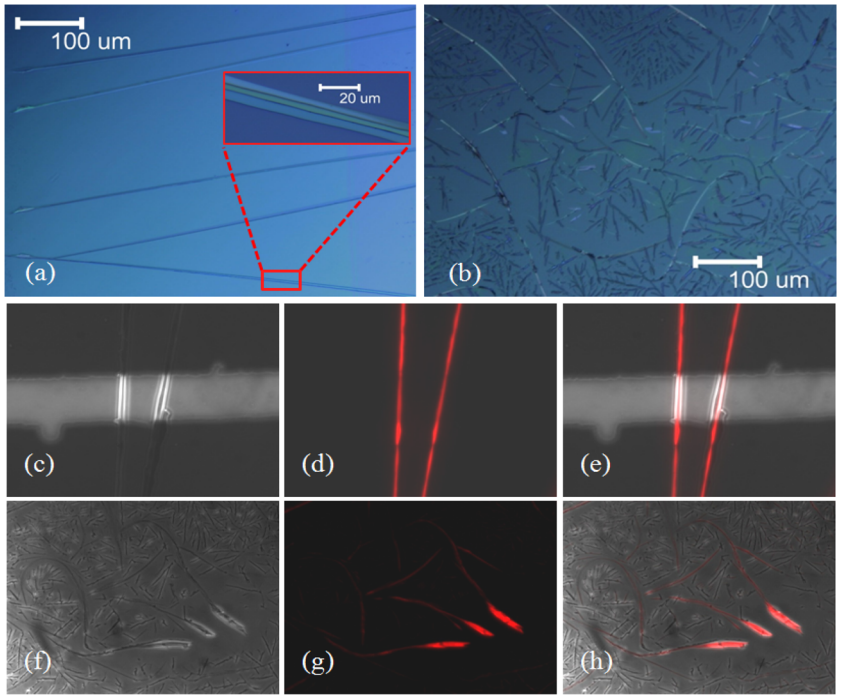


**Figure 2.** OM image of the crystals formed in presence (a) and in absence (b) of capillary tube. Images taken by CCD camera installed in a fluorescence microscope without (c, f) and with a rhodamine filter (d, g) and overlapped image (e, h) of the crystals formed in presence and in absence of capillary tube, respectively.

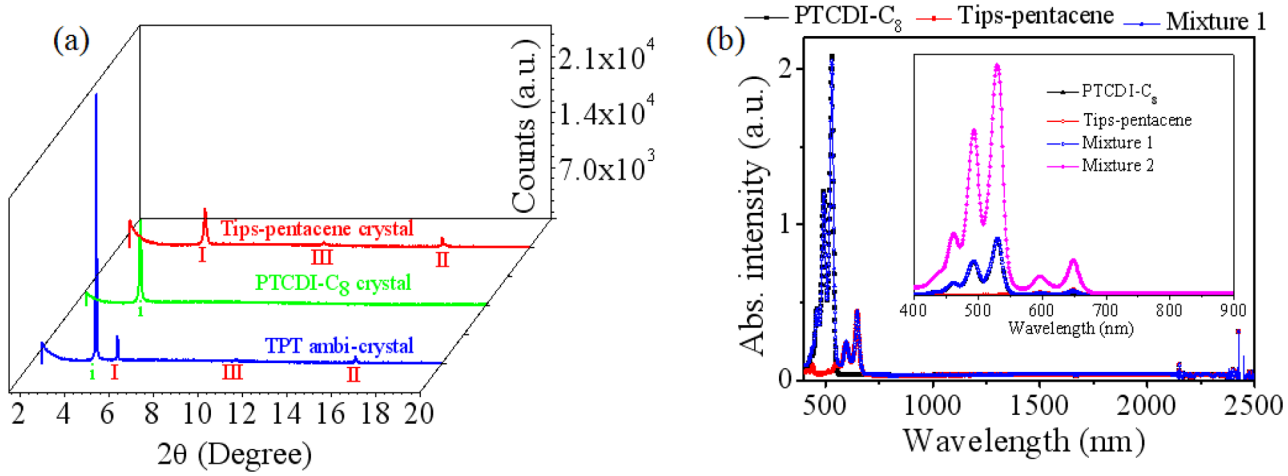


**Figure 3.** (a) XRD patterns of pure Tips-pentacene, pure PTCDI-$C_8$, and TPT-type ambipolar crystal. (b) The UV–visible-NIR absorption curves of pure PTCDI-$C_8$ (black line), Tips-pentacene (red line), and their mixture 1 (blue line) (1:7.5). The inset show UV–visible absorption curve of pure PTCDI-$C_8$ (black square), Tips-pentacene (red circle), and their mixtures (1:7.5). The absorption curves show characteristic peaks at 596 nm, 648 nm, and 463 nm for Tips-pentacene, and 493 nm, 530 nm for PTCDI-$C_8$. The mixtures show peaks at 461 nm, 493 nm, 530 nm, 598 nm, and 648 nm confirming the absence of charge transfer between Tips-pentacene and PTCDI-$C_8$. The concentration of Tips-pentacene and PTCDI-$C_8$ is $7.8 \times 10^{-4}$ M and $5.7 \times 10^{-3}$ M in mixture 1 and 0.014 and 0.1 M in mixture 2, respectively.

complexes show additional peaks, which are different from its parental compounds.[24]

The arrangement of the individual crystal within the TPT ambipolar crystal is investigated using polarized optical and fluorescent microscope images (with a rhodamine filter) of pure PTCDI-$C_8$ and Tips-pentacene crystals, as shown in Figure S2 (Supporting Information). Unlike the polarized optical microscope images of both semiconductor crystal (blue color), only PTCDI-$C_8$ crystal shows a sharp red color in fluorescent microscope images (but pure Tips-pentacene does not show any color). This fluorescent microscope technique with a rhodamine filter has been applied to the ambipolar crystals (obtained from 1:7.5 weight ratio solution) prepared in this study. Figure 2 shows images taken by CCD camera installed in a fluorescence microscope without [Figure 2c] and with a rhodamine filter [Figure 2d], and overlapped image [Figure 2e]. The overlapped images show bright red color only at the center of the crystal. This indicates that PTCDI-$C_8$ is located at the center of the ambipolar crystal and that Tips-pentacene is on the side of the PTCDI-$C_8$, which leads to TPT-type structure. The same fluorescence microscopic technique was also applied to the crystals formed in the absence of the

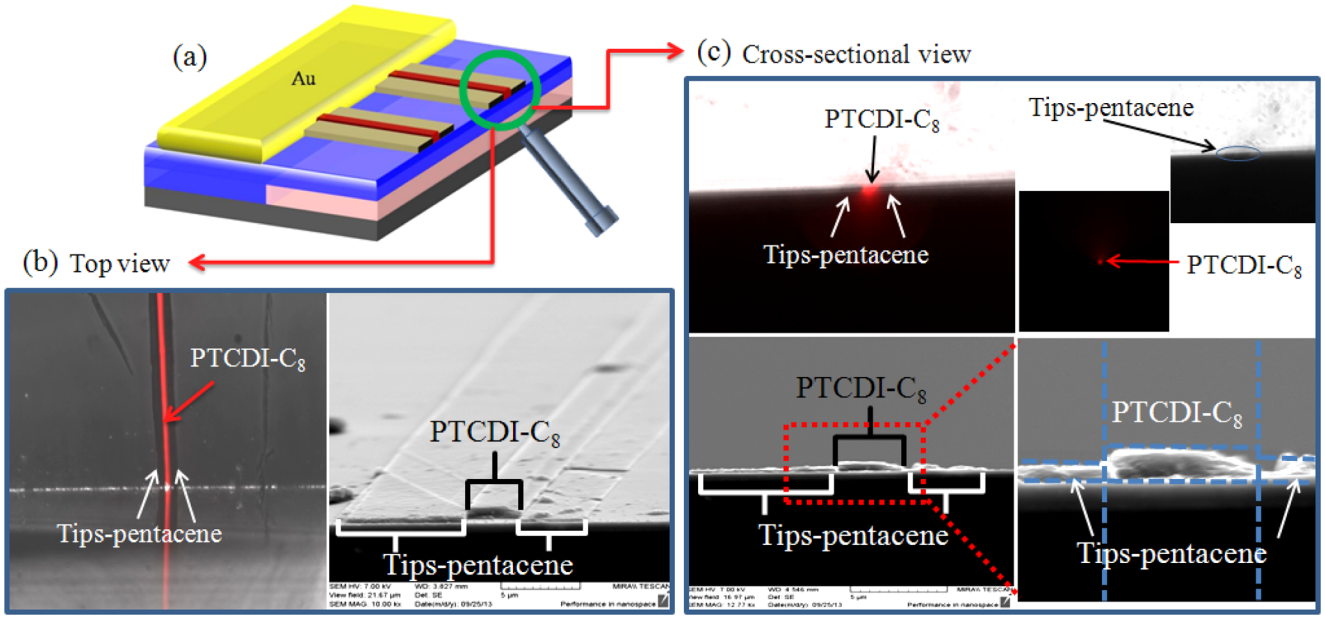


**Figure 4.** (a) Schematic diagram of the vertically cut device in the channel region (b) Fluorescent microscope image (left) and SEM image (right) of the vertically cut device from the top. A red line in the presence of a rhodamine filter indicated by a red arrow shows the presence of PTCDI-$C_8$, and the side dark lines indicated by white arrows indicate the presence of Tips-pentacene. (c) Cross-sectional FM images of the crystal (top). The red dots clearly indicate the PTCDI-$C_8$ crystal, and the black area on both sides of the dot indicated by white arrows show Tips-pentacene crystal. Cross-sectional SEM images (bottom) show the individual dimensions of crystal at various positions formed by PTCDI-$C_8$ and Tips-pentacene.

capillary, as shown in Figure 2(f–h). The formed crystals are randomly oriented and not in uniform shape. Hence, we found that our capillary tube method is highly useful and easy approach for the formation of highly directional unipolar and ambipolar crystals. Differential scanning calorimetry (DSC) analysis of the Tips-pentacene and PTCDI-$C_8$ also supports the formation of TPT-type ambipolar crystal. The endothermic melting onset and exothermic onset values for Tips-pentacene are 258 and 263 °C, respectively, similar to the literature value.[37] The respective endothermic melting onset and exothermic onset values for PTCDI-$C_8$ were also calculated from experiments as 227 and 189 °C, and their respective DSC curves are presented in Figure S3 (Supporting Information). The crystallization temperature for the two semiconductors is different, and hence, when the solution was allowed to crystallize, crystals of organic semiconductors may form one after another. Once the crystal is formed, the sides of the crystal provide thermodynamically more stable state for the formation of another crystal, leading to the formation of laterally stacked crystal in our system.

To date, most of the reported ambipolar crystals are based on charge transfer (CT) type complex,[20−24] which requires more complicated theory for device operation mechanism. Unlike the reported ambipolar crystals, our TPT crystal is not based on the CT complex, confirmed further by a ultraviolet visible near-infrared spectrometer.[24,38] The absorption spectra for the pure PTCDI-$C_8$ and Tips-pentacene, and the mixtures (at low and high concentration) is shown in Figure 3b. As shown in the figure, there is no additional peak in the spectrum of the mixture other than the peaks originated from the individual pure materials. An ambipolar system (DBTTF and TCNQ) reported by Wu et al.[24] shows a new absorption band appear in the range between 700 and 2100 nm originated from the formation of CT complex between DBTTF and TCNQ. However, in our system, there is no new absorption band in NIR region confirming the absence of charge transfer between PTCDI-$C_8$ and Tips-pentacene. There is no peak shift in UV–visible spectra at both dilute and concentrated mixed solution as shown in the inset of Figure 3b. It confirms further the absence of charge transfer between PTCDI-$C_8$ and Tips-pentacene.

The schematic structure of the vertically cut (at the channel area) ambi-OFET device based on TPT type ambipolar crystal is shown in Figures 4a. The structure was closely examined by top [Figure 4b] and cross-sectional [Figure 4c] scanning electron microscopy (SEM) and fluorescent microscopy images. Figure 4b shows a clear red line from the PTCDI-$C_8$ crystal along with a dark line from Tips-pentacene on both of its sides. At the edge of the vertically cut crystal, the intensity of the red color is quite high, and its reflection is seen. The cross-sectional fluorescent microscope image [Figure 4c] shows a red dot, indicating the presence of PTCDI-$C_8$ crystal in the center.

The top and cross-sectional fluorescent microscope images clearly demonstrate that the central portion of the ambipolar crystal is made up of PTCDI-$C_8$ and that the side part is Tips-pentacene. The top and cross-sectional SEM images show the shape and dimensions of the laterally stacked TPT type crystal. The individual widths of PTCDI-$C_8$ and Tips-pentacene crystal were calculated from the SEM image. The width of the Tips-pentacene crystal corresponding to the hole transport and PTCDI-$C_8$ crystal corresponding to the electron transport were calculated by the sum of the left and right parts of the crystal and the width of the central part as 11.7 and 3.9 $\mu$m, respectively.

Based on these results, we have fabricated OFETs with the crystal and analyzed their characteristics. The OFETs exhibit unipolar to ambipolar characteristics according to the weight ratio of Tips-pentacene to PTCDI-$C_8$, and the respective OFET results are summarized in Supporting Information Table S1. OFETs based on the crystal prepared from a 1:1 weight ratio

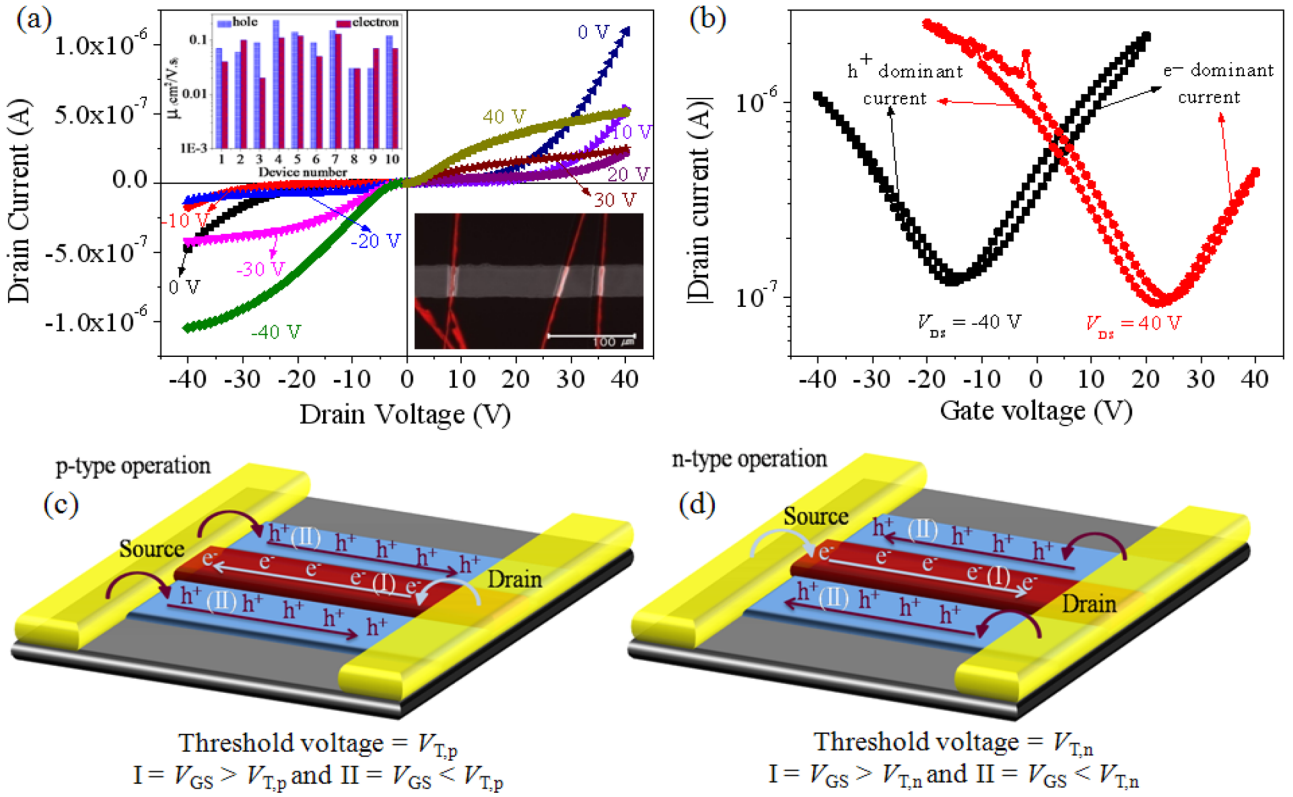


**Figure 5.** Output (a) and transfer (b) characteristics of ambi-OFETs with multiple ambipolar crystals. The inset shows the variation (top left) of the hole and electron mobilities obtained from ten devices and fluorescence microscopic image (bottom right) of the device with multiple crystals in the channel area. The scale bar of fluorescent microscope image is 100 $\mu$m. The charge injection and transport mechanism at various $V_{GS}$ and $V_{DS}$ for (c) p-type operation and (d) n-type operation.

show only n-type characteristics (confirmed by fabricating more than 5 devices) due to the PTCDI-$C_8$ (Supporting Information Figure S4).

The characteristics of the device based on the crystals from other weight ratios (1:2.5, 1:5, 1:7.5, and 1:10) were also studied. Devices based on the TP-type crystal prepared from a 1:2.5 solution show limited ambipolar transport behavior, as shown in Figures S5 and S6 (Supporting Information). OFETs based on crystals prepared from other solutions (1:5 and 1:10) show better ambipolar characteristics, as shown in Figures S7 and S8 (Supporting Information). Devices based on the crystal prepared from a 1:7.5 ratio solution show the best performance and well-balanced electron and hole transport behavior. Therefore, we have selected the TPT-crystal prepared from the 1:7.5 solution for a detailed study of ambi-OFETs.

The output ($I_{DS}$ vs $V_{DS}$) and transfer ($I_{DS}$ vs $V_{GS}$) characteristics of the ambi-OFET based on laterally stacked TPT type crystals (multi) from the 1:7.5 solution are shown in Figure 5(a and b, respectively), which clearly demonstrates ambipolar charge transport behavior. The fluorescent microscope image for the crystals present in the channel area is shown in the inset of Figure 5a. As shown in output characteristics of the OFETs Figure 5a, at low $V_{GS}$, an exponential increment of drain current was observed instead of saturation behavior. This is due to the flow of opposite charge carriers with increasing $V_{DS}$ on both sides (positive and negative $V_{DS}$ and $V_{GS}$). Upon further increasing the $V_{GS}$, the contribution of the current due to opposite charge carriers decreases, and typical n-type and p-type output characteristics are seen in the device at high positive and negative $V_{DS}$ and $V_{GS}$. Highly balanced saturation current by electrons and holes is achieved in the device with laterally stacked TPT type ambipolar crystals [Figure 5a].

Figure 5b shows the transfer curves of the ambi-OFETs with TPT-crystals in the channel. The drain current at $V_{DS} = -40$ V originated from hole carriers increases when $V_{GS} < -15$ V. On the other hand, when $V_{GS} > -15$ V, the increasing drain current is responsible for electron carriers. The best and average (measured from ten devices) field-effect hole mobility in p-channel operation was found to be 0.23 and 0.1 $cm^2/V{\cdot}s$, respectively. The similar transport behavior was observed during n-channel operation. For $V_{DS}$ = 40 V, the electron current is observed when $V_{GS} > 23$ V. When $V_{GS} < 23$ V, the increasing drain current may be responsible for hole transport. For this reason, the transfer curves at $V_{DS} = \pm 40$ V show V-shaped characteristics, confirming the efficient ambipolar behavior due to the presence of the laterally stacked TPT type ambipolar crystal in the channel area. Also, the best and average field-effect electron mobility in *n*-channel operation was estimated to be 0.13 and 0.07 $cm^2/V{\cdot}s$. Variation of electron and hole mobility of ten devices are depicted in the inset (top left) of Figure 5a.

The schematic charge injection and transport mechanism in our ambi-OFETs is shown in Figures 5(c and d) for p- and n-channel operation, respectively. The threshold voltage ($V_T$) of n-channel ($V_{T,n}$) and p-channel ($V_{T,p}$) operation plays an important role in the charge transport and can be expected to differ in ambipolar OFETs. For p-channel operation, both the gate and drain electrodes are negatively applied. In the lower negative $V_{GS}$ region ($V_{GS} > V_{T,p}$), $V_{GS}-V_{T,p}$ becomes positive,


dx.doi.org/10.1021/am5044505 | ACS Appl. Mater. Interfaces 2014, 6, 17804−17814

**Table 1. Performance of Ambi-OFETs Based on Multi, Two, and One TPT Crystal Prepared from a 1:7.5 Weight Ratio Solution**

| | $\mu_h$ ($cm^2$/V·s)[a] | | $\mu_e$ ($cm^2$/V·s)[b] | | $V_{Th}$ (V)[c] | | $I_{on}/I_{off}$ (V/dec)[d] | |
|---|---|---|---|---|---|---|---|---|
| no. of crystals | best | average | best | average | *p*-type | *n*-type | *p*-type | *n*-type |
| multi | 0.23 | 0.1 | 0.13 | 0.074 | −15 | 23 | $2.06 \times 10^{01}$ | $3.05 \times 10^{01}$ |
| two | 0.14 | 0.095 | 0.26 | 0.14 | −12.3 | 21.4 | $1.06 \times 10^{01}$ | $6.86 \times 10^{00}$ |
| one | 0.2 | 0.15 | 0.12 | 0.12 | −13 | 9 | $6.47 \times 10^{01}$ | $1.00 \times 10^{01}$ |

[a]Hole mobility. [b]Electron mobility. [c]Threshold voltage. [d]On to off current ratio.

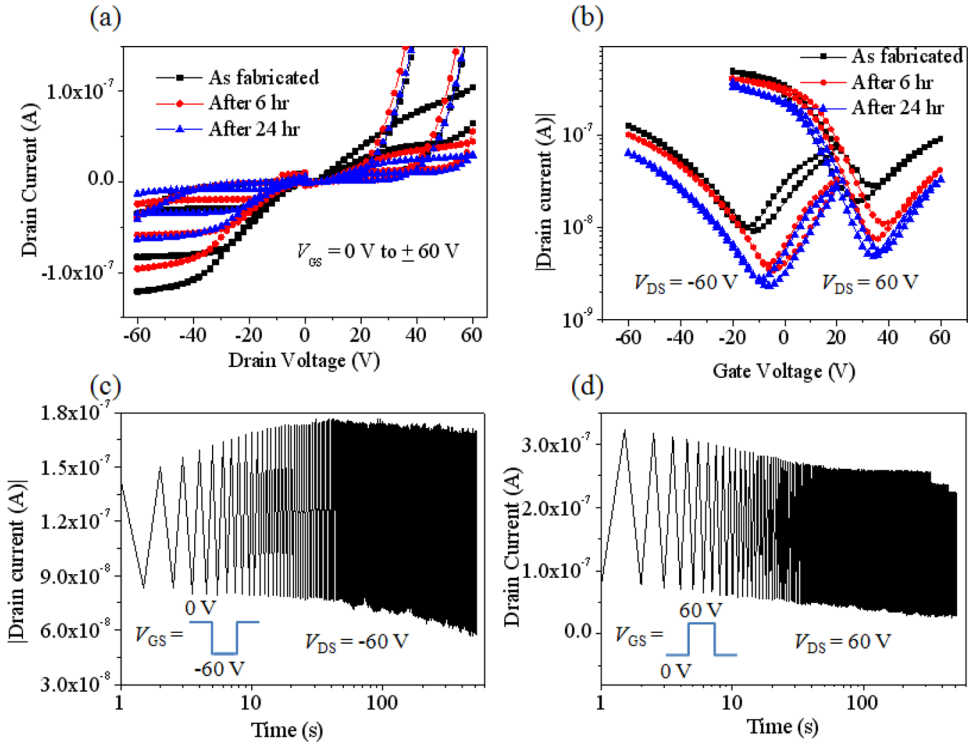


**Figure 6.** Long-term stability of the device. Output (a) and transfer (b) characteristics as a function of storage time in ambient conditions. Operational stability of the device during p-type operation (c) and n-type operation (d) for 500 cycles.

and the application of negative $V_{DS}$ generates a large driving force for electron injection to PTCDI-$C_8$ from the drain electrode rather than hole injection to Tips-pentacene from the source electrode, leading to electron current flow from the drain to the source [condition I, Figure 5c]. On the other hand, in the larger negative $V_{GS}$ region ($V_{GS} < V_{T,p}$), $V_{GS}-V_{T,p}$ becomes negative and leads to hole injection from the source to the Tips-pentacene, resulting in the flow of hole current from the source to the drain electrode [condition II, Figure 5c]. Similarly, for *n*-channel operation, in the lower positive $V_{GS}$ region ($V_{GS} < V_{T,n}$), hole current is observed due to injected holes from the drain electrode to Tips-pentacene [condition II, Figure 5d], and in the higher positive $V_{GS}$ region ($V_{GS} > V_{T,n}$) the electron current is observed due to injected electrons from the source electrode to PTCDI-$C_8$ [condition I, Figure 5d].

We can also control the crystal density by changing the concentration keeping the weight ratio constant and also successfully fabricated the two and one TPT-type crystal based Ambi-OFETs. These OFETs also show very good ambipolar charge transport in output and transfer characteristics, as shown in Figure S9(a and b) for two TPT crystals and Figure S9(c and d) (Supporting Information) for one TPT crystal. The transport mechanism can be understood in the same way. In the device with two TPT crystals, $V_{T,p}$ = −12.3 V and $V_{T,n}$ = 21.4 V are calculated, and typical hole-dominant and electron-dominant current characteristics are observed in the transfer characteristics with $V_{GS} < -12.3$ and $V_{GS} > 21.4$ V applied and at $V_{DS}$ = ± 40 V. The highest electron mobility value of 0.26 $cm^2$/V·s and hole mobility value of 0.14 $cm^2$/V·s have been achieved. Furthermore, the single TPT crystal based ambi-OFET also shows well-balanced charge transport behavior, as explained above. The charge carrier mobilities for electrons and holes in the one ambipolar crystal OFET are 0.12 $cm^2$/V·s and 0.2 $cm^2$/V·s with $V_{T,n}$ = 9 V and $V_{T,p}$ = −13 V for electron and hole transport, respectively. The performance parameters for multi, two, and one crystal based devices are summarized in Table 1.

To examine long-term and operational stability of the device in air, the device was repeatedly (after certain interval of time) biased by a drain-voltage ($V_{DS}$) sweep from 0 to −60 V and 0 to 60 V under a fixed gate-drain voltage ($V_{GS}$), biased from 0 to ±60 V with a step of ±20 V, respectively, and the corresponding output and transfer characteristic curves are shown in Figure 6(a and b, respectively). The devices show good operational stability even after 24 h (stored in ambient) with acceptable decrease in current and maintain relatively good electron and hole current balance. In addition, the dynamic stability of device based on the laterally stacked TPT type ambipolar crystal are also investigated and exhibited

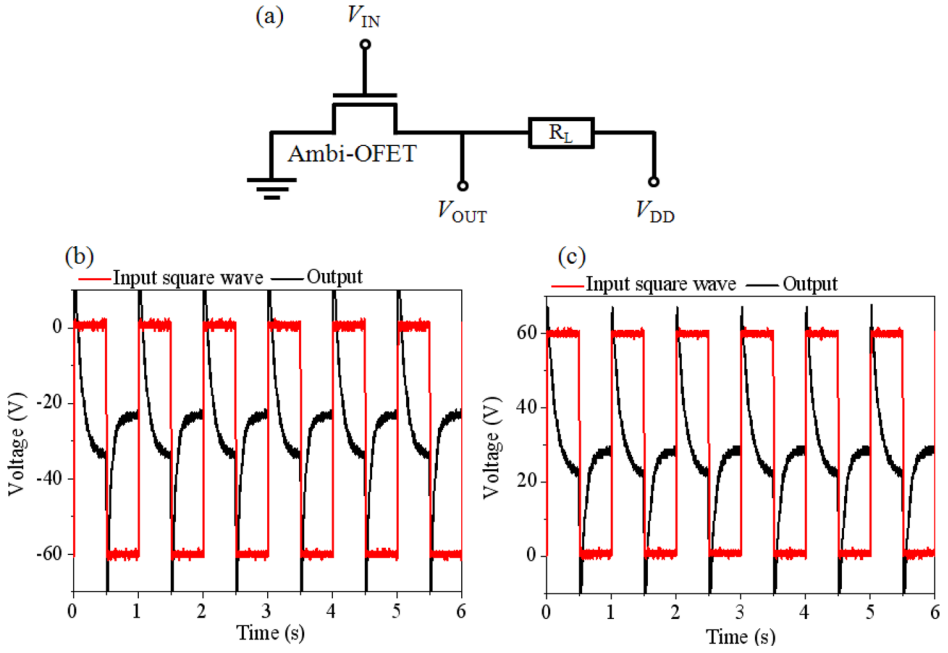


**Figure 7.** (a) Circuit diagram of the load type organic inverter based on ambi-OFET. 1 Hz input voltage signal (square, red) and output voltage response (black curve) of the inverter based on ambi-OFET and a 40 MΩ load resistor under the $V_{IN}$ switching between (b) 0 V and −60 V, $V_{DD}$ = −60 V, and (c) 0 and 60 V, $V_{DD}$ = 60 V.

excellent operating cyclic stability. The drain current was recorded by applying a constant $V_{DS}$ = −60 and 60 V and a square pulse of amplitude 0 to −60 V and 0 to 60 V to gate electrode with a frequency of 1 $H_Z$, and the dynamic switching response of the device are shown in Figure 6(c and d). The on and off currents driven by holes are stable throughout the scan period, but on and off currents due to electrons decreased slightly. Overall, the devices maintained on- and off-currents without significant degradation during 500 turn-on and -off cycles. These results indicate that laterally stacked TPT type ambipolar crystal-based device had significantly good stability in ambient conditions and under continuous bias stress.

After the fabrication and analysis of ambi-OFETs based on the ambipolar TPT crystals, we constructed a load- and complementary-type inverter by employing an ambi-OFET based on multi TPT type crystal obtained from a 1:7.5 weight ratio solution. A schematic representation of the constructed load-type inverter is shown in Figure 7a. The transient response of the inverter was recorded by applying a square wave input voltage signal (switching between 0 to −60 V and 0 to +60 V) with 1 $H_Z$ frequency while $V_{DD}$ was kept at −60 V and +60 V. As can be seen in Figure 7(b and c), under the switching frequency of 1 Hz, the output voltage switched with delay in the signal, and the device shows PMOS-like and NMOS-like characteristics, respectively. Rising ($t_r$) and falling ($t_f$) times with spikes are obtained as 148 and 197 ms for PMOS and as 121 and 160 ms for NMOS-like load-type organic inverters, respectively. This delay in the response time is attributed to the overlapped capacitance in our device structure. If the gate electrode was well optimized, better dynamic response could be obtained.

Finally, complementary-like inverters were fabricated using two ambi-OFETs, and the schematic diagram for complementary-like inverters is represented in Figure 8a. The output and transfer characteristic curves of ambi-OFETs incorporated in the CMOS-like inverter show well-balanced charge transport behavior and are shown in Figure S10 (Supporting Information). The static and dynamic responses of the CMOS-like inverter based on the ambi-OFETs have been analyzed. The voltage transfer characteristics of the CMOS-like inverter are depicted in Figure 8b, which shows good inversion characteristics in $V_{OUT}$. As in other complementary-like organic inverters based on ambi-OFETs, this inverter shows switching performance in the first and third quadrants with ± $V_{DD}$ and ± $V_{IN}$ applied in the presence of both types of semiconducting materials in the crystal in the channel region.

A sharp inversion is found near 35.9 and 38.1 V in forward and reverse cycles with a voltage of $V_{DD}$ = 60 V applied to the inverter. The voltage gain (absolute value of $dV_{OUT}/dV_{IN}$) was calculated from the voltage transfer curves and reached maximum values of 10.7 and 9.7 in the forward and reverse scans, respectively, as shown in the inset of Figure 8b (top-left panels). Similarly, with a supplied voltage of $V_{DD}$ = −60 V, the device also shows inversion characteristics in the third quadrant, and the inversion voltages are −20.9 V and −21.0 V in the forward and reverse scans with gain values of 9.02 and 9.63 (inset of Figure 8b bottom-right panel), respectively.

The respective noise margin high ($NM_H$) and noise margin low ($NM_L$) values were also calculated from the voltage transfer characteristics of the device in forward and reverse bias by applying $V_{DD}$ = ± 60 V. When $V_{DD}$ = 60 V is applied, the values of noise margin at high and low voltages are 20.17 and 32.86 V in forward bias, while they are 17.13 and 34.49 V in reverse bias, respectively. Similarly, when $V_{DD}$ = −60 V is applied, the values are −35.11 and −15.63 V in forward bias and −34.87 and −18.67 V in reverse bias, respectively.

The logic threshold voltage ($V_M$), gain, and noise margin of the CMOS-like inverter are summarized in Table 2. The typical dynamic response of the CMOS-like organic inverter at constant $V_{DD}$ is presented in Figure 8(c and d), which demonstrate decent inversion characteristics, while $V_{DD}$ was kept at −60 V and +60 V, respectively. As shown in $V_{OUT}$, the device clearly shows inversion in the applied $V_{IN}$ swept between 0 to −40 V and 0 to +40 V, respectively. This clearly indicates

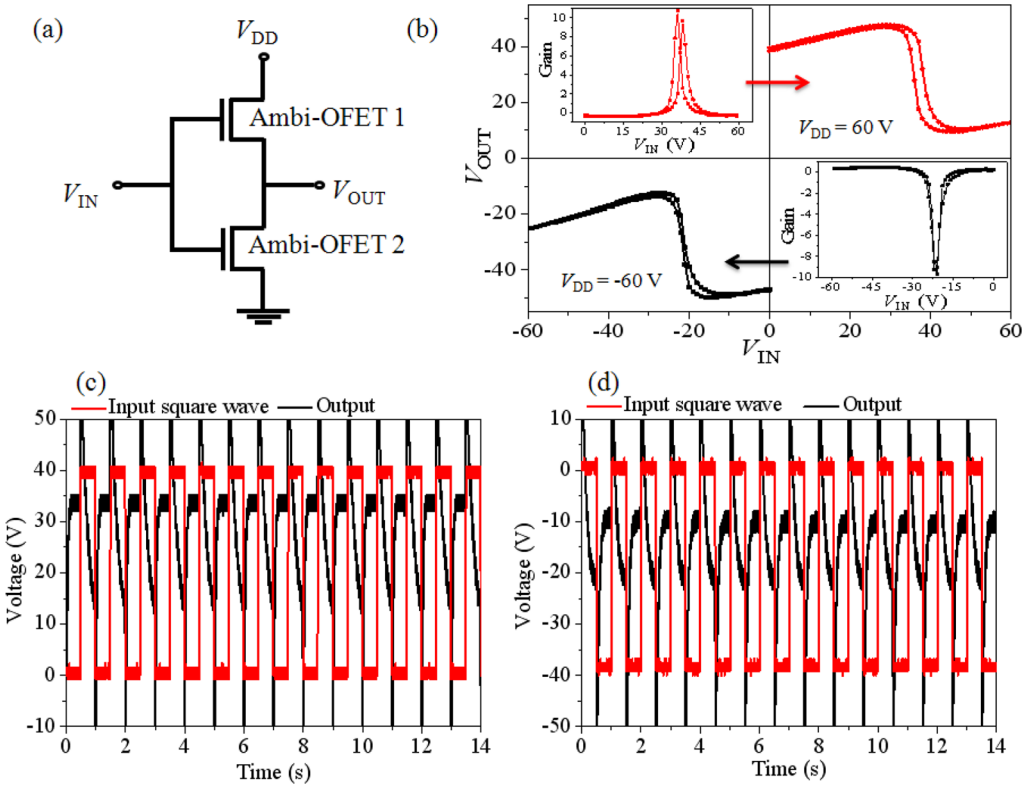


**Figure 8.** (a) Circuit diagram of the CMOS-like inverter based on two ambi-OFETs. (b) Transfer characteristics of CMOS-like organic inverter at the supply voltage $V_{DD}$ = 60 V (1st quadrant) and $V_{DD}$ = −60 V (3rd quadrant). The inset indicates gain of the inverter. A 1 Hz input voltage signal (square red) and output voltage response (black) of the CMOS-like inverter under the $V_{IN}$ switching between (c) 0 and 40 V at $V_{DD}$ = 40 V and (d) 0 V and −40 V at $V_{DD}$ = −40 V.

**Table 2. Summary of Performance of CMOS-like Inverter Using Two Ambi-OFETs**

| | $V_M$ (V)[a] | gain | $NM_H$[b] | $NM_L$[c] |
|---|---|---|---|---|
| $V_{DD}$ = +60 V forward | 35.9 | 10.7 | 20.2 | 32.9 |
| $V_{DD}$ = +60 V reverse | 38.1 | 9.7 | 17.1 | 34.5 |
| $V_{DD}$ = −60 V forward | −20.9 | 9.0 | 35.1 | 15.9 |
| $V_{DD}$ = −60 V reverse | −21.0 | 9.6 | 34.9 | 18.7 |

[a]Logic threshold voltage. [b]Noise margin high. [c]Noise margin low.

that the CMOS-like organic inverter based on ambi-OFETs with the TPT type ambipolar crystal shows well-balanced static and dynamic characteristics. The rising ($t_r$) and falling ($t_f$) times of $V_{OUT}$ were obtained as 191 and 154 ms, respectively. A similar study on the CMOS-like inverter with ambi-OFETs based on an ambipolar TPT crystal prepared from a 1:5 weight ratio solution has also been done, and the characteristics are shown in Figures S11−S13 and summarized in Table S2 (Supporting Information).

## CONCLUSION

We prepared laterally stacked TPT type ambipolar crystal through a solution process using Tips-pentacene and PTCDI-$C_8$ as p- and n-type organic semiconductors, respectively. OFETs with ambipolar electrical response were fabricated using the TPT-crystals, and their characteristics were investigated. The solution-processed ambipolar crystal-based OFETs show appreciable ambipolar charge carrier transport performance with hole and electron mobilities as high as 0.2 $cm^2/V{\cdot}s$. Without charge transfer between the materials, the molecules could be self-assembled to form laterally stacked TPT type crystal containing both polarities. In addition, a CMOS-like inverter was fabricated by connecting the two ambipolar OFETs. The organic inverter shows well-balanced static and dynamic characteristics. The unique structure of the ambipolar crystal in which both the semiconductors are in direct contact with electrodes opens a new and versatile route toward highly efficient ambipolar miniaturized organic electronic devices. This simple solution-based approach for the fabrication of ambipolar organic electronic devices could be extended to other organic molecules to broaden its applicability.

## ASSOCIATED CONTENT

### Supporting Information

Polarized optical microscope and fluorescent microscope images of the crystals. DSC thermograms of Tips-pentacene and PTCDI-$C_8$. Output and transfer characteristics of the OFETs, voltage transfer characteristics, and gain curves of CMOS-like organic inverter. This material is available free of charge via the Internet at http://pubs.acs.org

## AUTHOR INFORMATION

### Corresponding Author

*Email: pyosm@konkuk.ac.kr.

### Author Contributions

†Amit Kumar and Hyunseok Shim contributed equally to this work. All authors have given approval to the final version of the manuscript.

### Notes

The authors declare no competing financial interest.

## ■ ACKNOWLEDGMENTS

This work was supported by the National Research Foundation (NRF) funded by the Korean government (MEST) (2012R1A2A2A01045694).

## ■ REFERENCES

(1) Di, C.-A.; Yu, G.; Liu, Y.; Xu, X.; Wei, D.; Song, Y.; Sun, Y.; Wang, Y.; Zhu, D. Organic Light-Emitting Transistors Containing a Laterally Arranged Hetero-Junction. *Adv. Funct. Mater.* **2007**, *17*, 1567−1573.

(2) Yomogida, Y.; Sakai, H.; Sawabe, K.; Gocho, S.; Bisri, S. Z.; Nakanotani, H.; Adachi, C.; Hasobe, T.; Iwasa, Y.; Takenobu, T. Multi-Color Light-Emitting Transistors Composed of Organic Single Crystals. *Org. Electron.* **2013**, *14*, 2737−2742.

(3) Anthopoulos, T. D.; Setayesh, S.; Smits, E.; Cölle, M.; Cantatore, E.; Boer, B. D.; Blom, P. W. M.; Leeuw, D. M. D. Air-Stable Complementary-like Circuits Based on Organic Ambipolar Transistors. *Adv. Mater.* **2006**, *18*, 1900−1904.

(4) Mohebbi, A. R.; Yuen, J.; Fan, J.; Munoz, C.; Wang, M. F.; Shirazi, R. S.; Seifter, J.; Wudl, F. Emeraldicene as an Acceptor Moiety: Balanced-Mobility, Ambipolar, Organic Thin-Film Transistors. *Adv. Mater.* **2011**, *23*, 4644−4648.

(5) Etschel, S. H.; Waterloo, A. R.; Margraf, J. T.; Amin, A. Y.; Hampel, F.; Jager, C. M.; Clark, T.; Halik, M.; Tykwinski, R. R. An Unsymmetrical Pentacene Derivative with Ambipolar Behavior in Organic Thin-Film Transistors. *Chem. Commun.* **2013**, *49*, 6725−6727.

(6) Imai, S.; Yanagi, H.; Hotta, S. Ambipolar Field-Effect Transistors with Bilayered Thiophene/Phenylene Co-Oligomers. *Org. Electron.* **2013**, *14*, 80−85.

(7) Jea, M.; Kumar, A.; Cho, H.; Yang, D.; Shim, H.; Palai, A. K.; Pyo, S. An Organic Microcrystal Array-Embedded Layer: Highly Directional Alternating p- and n-Channels for Ambipolar Transistors and Inverters. *J. Mater. Chem. C* **2014**, *2*, 3980−3987.

(8) Wang, H.; Yan, D. Organic Heterostructures in Organic Field-Effect Transistors. *NPG Asia Mater.* **2010**, *2*, 69−78.

(9) Meijer, E. J.; Leeuw, D. M. D.; Setayesh, S.; Veenendaal, E. V.; Huisma, B.-H.; Blom, P. W. M.; Hummelen, J. C.; Scherf, U.; Klapwijk, T. M. Solution-processed Ambipolar Organic Field-Effect Transistors and Inverters. *Nat. Mater.* **2003**, *2*, 678−682.

(10) Yang, S. H.; Cho, M. Y.; Jo, S. G.; Jung, J. S.; Jung, K. H.; Bae, S. Y.; Choi, D. H.; Kim, S.; Joo, J. Photoresponsive Ambipolar Transport Characteristics of Organic Thin Film Transistors using Soluble HB-ant-THT and PCBM Composites. *Synth. Met.* **2012**, *162*, 332−336.

(11) Ahn, K.; Kim, J. B.; Park, H.; Kim, H.; Lee, M. H.; Kim, B. J.; Cho, J. H.; Kang, M. S.; Lee, D. R. Enhancing Crystallinity of $C_{60}$ Layer by Thickness-Control of Underneath Pentacene Layer for High Mobility $C_{60}$/Pentacene Ambipolar Transistors. *Appl. Phys. Lett.* **2013**, *102*, 043306.

(12) Wang, J.; Wang, H. B.; Yan, X. J.; Huang, H. C.; Jin, D.; Shi, J. W.; Tang, Y. H.; Yan, D. H. Heterojunction Ambipolar Organic Transistors Fabricated by a Two-Step Vacuum-Deposition Process. *Adv. Funct. Mater.* **2006**, *16*, 824−830.

(13) Chang, J.-F.; Gwinner, M. C.; Caironi, M.; Sakanoue, T.; Sirringhaus, H. Conjugated-Polymer-Based Lateral Heterostructures Defined by High-Resolution Photolithography. *Adv. Funct. Mater.* **2010**, *20*, 2825−2832.

(14) Shi, J.; Wang, H.; Song, D.; Tian, H.; Geng, Y.; Yan, D. n-Channel, Ambipolar, and p-Channel Organic Heterojunction Transistors Fabricated with Various Film Morphologies. *Adv. Funct. Mater.* **2007**, *17*, 397−400.

(15) Ferraris, J. P.; Poehler, T. O.; Bloch, A. N.; Cowan, D. O. Synthesis of the Highly Conducting Organic Salt: Tetramethyltetrathiofulvalenium-Tetracyano-*p*-Quinodimethanide. *Tetrahedron Lett.* **1973**, *14*, 2553−2556.

(16) Bag, P.; Pal, S. K.; Itkis, M. E.; Sarkar, A.; Tham, F. S.; Donnadieu, B.; Haddon, R. C. Synthesis of Tetrachalcogenide-Substituted Phenalenyl Derivatives: Preparation and Solid-State Characterization of Bis(3,4,6,7-Tetrathioalkyl-Phenalenyl)Boron. *J. Am. Chem. Soc.* **2013**, *135*, 12936−12939.

(17) Tayi, A. S.; Shveyd, A. K.; Sue, A. C.-H.; Szarko, J. M.; Rolczynski, B. S.; Cao, D.; Kennedy, T. J.; Sarjeant, A. A.; Stern, C. L.; Paxton, W. F.; Wu, W.; Dey, S. K.; Fahrenbach, A. C.; Guest, J. R.; Mohseni, H.; Chen, L. X.; Wang, K. L.; Stoddart, J. F.; Stupp, S. I. Room-Temperature Ferroelectricity in Supramolecular Networks of Charge-Transfer Complexes. *Nature* **2012**, *488*, 485−489.

(18) Mori, T. Organic Charge-Transfer Salts and the Component Molecules in Organic Transistors. *Chem. Lett.* **2011**, *40*, 428−434.

(19) Sakai, M.; Sakuma, H.; Ito, Y.; Saito, A.; Nakamura, M.; Kudo, K. Ambipolar Field-Effect Transistor Characteristics of (BEDT-TTF)(TCNQ) Crystals and Metal-like Conduction Induced by a Gate Electric Field. *Phys. Rev. B* **2007**, *76*, 045111.

(20) Zhu, L.; Yi, Y.; Li, Y.; Kim, E.-G.; Coropceanu, V.; Brédas, J.-L. Prediction of Remarkable Ambipolar Charge-Transport Characteristics in Organic Mixed-Stack Charge-Transfer Crystals. *J. Am. Chem. Soc.* **2012**, *134*, 2340−2347.

(21) Park, S. K.; Varghese, S.; Kim, J. H.; Yoon, S.-J.; Kwon, O. K.; An, B.-K.; Gierschner, J.; Park, S. Y. Tailor-Made Highly Luminescent and Ambipolar Transporting Organic Mixed Stacked Charge-Transfer Crystals: An Isometric Donor−Acceptor Approach. *J. Am. Chem. Soc.* **2013**, *135*, 4757−4764.

(22) Zhang, J.; Tan, J.; Ma, Z.; Xu, W.; Zhao, G.; Geng, H.; Di, C.; Hu, W.; Shuai, Z.; Singh, K.; Zhu, D. Fullerene/Sulfur-Bridged Annulene Co-Crystals: Two-Dimensional Segregated Heterojunctions with Ambipolar Transport Properties and Photoresponsivity. *J. Am. Chem. Soc.* **2013**, *135*, 558−561.

(23) Zhang, J.; Geng, H.; Virk, T. S.; Zhao, Y.; Tan, J.; Di, C.-a.; Xu, W.; Singh, K.; Hu, W.; Shuai, Z.; Liu, Y.; Zhu, D. Sulfur-Bridged Annulene-TCNQ Co-Crystal: A Self-Assembled "Molecular Level Heterojunction" with Air Stable Ambipolar Charge Transport Behavior. *Adv. Mater.* **2012**, *24*, 2603−2607.

(24) Wu, H.-D.; Wang, F.-X.; Xiao, Y.; Pan, G.-B. Preparation and Ambipolar Transistor Characteristics of Co-Crystal Microrods of Dibenzotetrathiafulvalene and Tetracyanoquinodimethane. *J. Mater. Chem. C* **2013**, *1*, 2286−2289.

(25) Sakai, M.; Sakum, H.; Ito, Y.; Saito, A.; Nakamura, M.; Kudo, K. Ambipolar Field-Effect Transistor Characteristics of (BEDT-TTF)(TCNQ) Crystals and Metal-like Conduction Induced by a Gate Electric Field. *Physical Rev. B* **2007**, *76*, 045111.

(26) Wakahara, T.; D'Angelo, P.; Miyazawa, K.; Nemoto, Y.; Ito, O.; Tanigaki, N.; Bradley, D. D.C.; Anthopoulos, T. D. Fullerene/Cobalt Porphyrin Hybrid Nanosheets with Ambipolar Charge Transporting Characteristics. *J. Am. Chem. Soc.* **2012**, *134*, 7204−7206.

(27) Hasegawa, T.; Mattenberger, K.; Takeya, J.; Batlogg, B. Ambipolar Field-Effect Carrier Injections in Organic Mott Insulators. *Phys. Rev. B* **2004**, *69*, 245115.

(28) Takahashi, Y.; Hasegawa, T.; Abe, Y.; Tokura, Y.; Nishimura, K.; Saito, G. Tuning of Electron Injections for n-Type Organic Transistor Based on Charge-Transfer Compounds. *Appl. Phys. Lett.* **2005**, *86*, 063504.

(29) Takahashi, Y.; Hasegawa, T.; Abe, Y.; Tokura, Y.; Saito, G. Organic Metal Electrodes for Controlled p- and n-Type Carrier Injections in Organic Field-Effect Transistors. *Appl. Phys. Lett.* **2006**, *88*, 073504.

(30) Tang, Q.; Tong, Y.; Li, H.; Ji, Z.; Li, L.; Hu, W.; Liu, Y.; Zhu, D. High-Performance Air Stable Bipolar Field-Effect Transistors of Organic Single-Crystalline Ribbons with an Air−Gap Dielectric. *Adv. Mater.* **2008**, *20*, 1511−1515.

(31) Mukherjee, B.; Mukherjee, M.; Sim, K.; Pyo, S. M. Solution Processed, Aligned Arrays of TCNQ Microcrystals for Low-Voltage Organic Phototransistor. *J. Mater. Chem.* **2011**, *21*, 1931−1936.

(32) Palai, A. K.; Lee, J.; Das, S.; Lee, J.; Cho, H.; Park, S. U.; Pyo, S. M. A Diketopyrrolopyrrole Containing Molecular Semiconductor: Synthesis, Characterization, and Solution-Processed 1D-Microwire Based Electronic Devices. *Org. Electron.* **2012**, *13*, 2553−2560.

(33) Mukherjee, B.; Sim, K.; Shin, T. J.; Lee, J.; Mukherjee, M.; Ree, M.; Pyo, S. Organic Phototransistors Based on Solution Grown,

Ordered Single Crystalline Arrays of a π-Conjugated Molecule. *J. Mater. Chem.* **2012**, *22*, 3192−3200.
(34) Palai, A. K.; Lee, J.; Shin, T. J.; Kumar, A.; Park, S.-U.; Pyo, S. M. Solution-Grown Single-Crystalline Microwires of a Molecular Semiconductor with Improved Charge Transport Properties. *Chem. Commun.* **2014**, *50*, 8845−8848.
(35) Madec, M.-B.; Crouch, D.; Llorente, G. R.; Whittle, T. J.; Geoghegan, M.; Yeates, S. G. Organic Field Effect Transistors from Ambient Solution Processed Low Molar Mass Semiconductor-Insulator Blends. *J. Mater. Chem.* **2008**, *18*, 3230−3236.
(36) Karak, S.; Ray, S. K.; Dhar, A. Photo induced Charge Transfer and Photovoltaic Energy Conversion in Self-Assembled N,N-Dioctyl-3,4,9,10-Perylenedicarboximide Nano-Ribbons. *Appl. Phys. Lett.* **2010**, *97*, 043306.
(37) *Pentacene Data Sheet*; Ossila Ltd.: Sheffield, 2009−2014. http://www.ossila.com/support/TIPS_Pentacene_Data_Sheet.php.
(38) Yu, W.; Wang, X.-Y.; Li, J.; Li, Z.-T.; Yan, Y.-K.; Wang, W.; Pei, J. A Photoconductive Charge-Transfer Crystal with Mixed-Stacking Donor−Acceptor Heterojunctions within the Lattice. *Chem. Commun.* **2013**, *49*, 54−56.